Published in final edited form as:
Magn Reson Med. 2008 November ; 60(5): 1178–1189. doi:10.1002/mrm.21810.

Focal Reversible Deactivation of Cerebral Metabolism Affects Water Diffusion

Mark H. Khachaturian[1,2,*], **John Arsenault**[1,2,3,4], **Leeland B. Ekstrom**[1,2,3], **David S. Tuch**[1,3], and **Wim Vanduffel**[1,4]

[1]Athinoula A. Martinos Center for Biomedical Imaging, Massachusetts General Hospital, Harvard Medical School, Charlestown, Massachusetts.

[2]Department of Nuclear Science and Engineering, Massachusetts Institute of Technology, Cambridge, Massachusetts.

[3]Harvard-MIT Division of Health Sciences and Technology, Massachusetts Institute of Technology, Cambridge, Massachusetts.

[4]Laboratorium voor Neuro-en Psychofysiologie, Katholieke Universiteit Leuven, Campus Gasthuisberg, Leuven, Belgium.

Abstract

The underlying biophysical mechanisms which affect cerebral diffusion contrast remain poorly understood. We hypothesized that cerebral metabolism may affect cerebral diffusion contrast. The purpose of this study was to develop the methodology to reversibly deactivate cerebral metabolism and measure the effect on the diffusion MRI signal. We developed an MRI-compatible cortical cooling system to reversibly deactivate cortical metabolism in rhesus monkey area V1 and used MR thermometry to calculate three-dimensional temperature maps of the brain to define the extent of deactivated brain in vivo. Significant changes in the apparent diffusion coefficient (ADC) were *only* observed during those experiments in which the cortex was cooled below the metabolic cutoff temperature of 20°C. ADC decreases (12–20%) were observed during cortical cooling in regions where the temperature did not change. The normalized in vivo ADC as function of temperature was measured and found to be equivalent to the normalized ADC of free water at temperatures above 20° C, but was significantly decreased below 20°C (20–25% decrease). No changes in fractional anisotropy were observed. In future experiments, we will apply this methodology to quantify the effect of reversible deactivation on neural activity as measured by the hemodynamic response and compare water diffusion changes with hemodynamic changes.

Keywords

diffusion MRI; cerebral metabolism; reversible deactivation; cooling; MR thermometry; ADC; FA

Diffusion MRI measures the Brownian motion of water molecules in brain tissue on length scales ranging from 10 nm to 100 μm, and on time scales ranging from 1 ms to 1 s (1). Given that the average size of neurons in the brain is approximately 10 μm, diffusion MRI provides a sensitive probe of tissue microstructure. Diffusion MRI has emerged as a powerful tool to

*Correspondence to: Mark H. Khachaturian, Athinoula A. Martinos Center for Biomedical Imaging, Massachusetts General Hospital, 149 13th Street, Room 2301, Charlestown, Massachusetts 02129. markk@nmr.mgh.harvard.edu.
Dr. Tuch's present address is Novartis Pharma AG, Switzerland.

investigate a wide range of neuropathologies such as stroke, Parkinson's disease, HIV dementia, schizophrenia, cocaine addiction, normal aging, Alzheimer's disease, chronic alcoholism, multiple sclerosis, epilepsy, and amyotrophic lateral sclerosis (2,3). More recently, diffusion MRI has also been proposed as a promising technique to identify anatomical white-matter fiber tracts in vivo (4–7) and even to measure neural activity (8).

In clinical diffusion MRI, the two scalar measures of diffusion in cerebral tissue are the apparent diffusion coefficient (ADC) and fractional anisotropy (FA). The ADC represents the magnitude of diffusion, whereas the FA is a measure of its anisotropy. Despite the widespread applications and usefulness of diffusion MRI in basic and clinical neuroscience, the underlying biophysical mechanisms which affect diffusion contrast (ADC and FA) remain largely unknown (9).

Initially, it had been assumed that FA in cerebral white matter was caused by the diffusion barrier presented by the myelin sheath. However, diffusion anisotropy has been observed in de-myelinated garfish nerve (10), premyelinated newborn white matter (11), cortical gray matter in rat (12), and the thalamus (13). Furthermore, FA changes in ischemia studies have been shown to occur over longer time periods (hours to days) and after lesions causing anterograde and retrograde secondary white matter degeneration (14,15).

A recent study suggested that ADC depends on neuronal activity (8). It has also been suggested that the ADC of water decreased during the inhibition of fast axonal transport (10). Another study in which microtubule concentration was depleted found no affect on the ADC (16). Yet, the latter experiments were confounded by crystal formation during the artificial breakdown of microtubule, which could have affected the ADC. Because of the immediate decrease in ADC during (i) ischemia, (ii) spreading depression, (iii) inhibition of fast axonal transport (10), (iv) and changes during neuronal activity (8), we hypothesized that processes directly dependent on cerebral metabolism affect the ADC.

The purpose of this study is to describe the methodology that we developed to focally reversibly deactivate cerebral metabolism and measure the diffusion MRI signal. By focally deactivating cerebral metabolism in a reversible manner, the relationship between the diffusion MRI signal and one aspect of neural activity, the fMRI response, can be quantified throughout the brain. A later study will discuss the application of this methodology to study the effect of reversible deactivation on the hemodynamic response. Monkeys were chosen instead of rats because of the future desire to compare the ADC with the hemodynamic response in visual cortex.

To reversibly deactivate the cortex, we developed an MRI-compatible cortical cooling probe. Indeed, it is well-established that cooling cortical tissue below 20°C blocks metabolism, hence also neuronal activity (17–20). By reversibly deactivating cerebral metabolism, rather than making permanent lesions or inducing stroke, we avoided confounding mechanisms that could contribute to the diffusion signal as observed during neuropathology, such as functional and anatomical reorganization (plasticity), blood accumulation, macrophage infusion, gliosis, and necrosis. Marked cooling could also have an ischemic effect and ADC decreases would be expected in the deactivation region. In deoxyglucose (DG) studies, DG uptake decreased in foci connected with the deactivated site which would could also cause ADC decreases outside the deactivation region (21).

Hitherto, it has been difficult to quantify in vivo the degree and three-dimensional (3D) extent of brain tissue affected during reversible deactivation experiments, irrespective of the method used (e.g., cortical cooling or drug injection). To overcome this problem, we measured the temperature of the brain inside the MR-scanner using proton resonance frequency shift thermometry (PRFST) (22,23). To assess the accuracy and precision of the PRFST method, we compared ex vivo MR thermometry measurements with concurrent temperature measurements using MRI-compatible thermocouples. The PRFST method allowed us to

calculate 3D temperature maps (isothermals) at a temporal resolution of four seconds and infer the amount of affected cortex during a cooling experiment. A potential confound during combined cooling-DTI experiments is the temperature dependence of ADC, such that a change in the ADC may simply reflect a change in temperature. However, the in vivo 3D temperature maps allowed us to quantify precisely ADC changes in voxels where the temperature did not change.

Another potential confound of this study is that cooling will induce a physiological response in the local vasculature (i.e., blood flow) so that a change in ADC could not be attributed solely to changes in metabolism (24). Although the authors believe that the small volume fraction of blood in cerebral tissue, ~5% (25,26), could not be responsible for the changes in diffusion observed, the quantification of changes in blood flow during deactivation was not measured directly and warrants investigation.

In summary, we were able to reversibly deactivate cerebral metabolism in a small portion of macaque V1 in a MRI-compatible manner. Moreover, we were able to define dynamically the extent of this deactivation. Short-term deactivations (~30 min) led to pronounced changes in ADC, but not FA, in voxels at distant sites from the deactivated region where the temperature had not changed. These data suggest that a considerable fraction of the ADC in the brain depends on normal cerebral metabolism.

METHODS

Animals

MRI data were acquired from three juvenile male rhesus monkeys (*Macaca mulatta*, weighing 5.5 kg [M1] and 4.2 kg [M2], 6.2 kg [M3]). A 0.75-inch-diameter recording well (Crist Instruments, Washington, DC) was placed over V1 of the right hemisphere. The recording well exposed the dura and was sealed with a cap when the monkey was not in the scanner. The data were acquired on a Siemens Allegra (M1) and Trio (M2) 3T MRI scanner located at the Athinoula A. Martinos Center for Biomedical Imaging, Massachusetts General Hospital (Charlestown, Massachusetts). All procedures conformed to Massachusetts General Hospital and National Institutes of Health guidelines for the care and use of laboratory animals (Subcommittee on Research Animal Care protocol #2003N000338). The animal was anesthetized with a ketamine and xylazine mixture (induction 10 and 0.5 mg/kg, i.m., maintenance with 0.5 mg/kg ketamine every 30 min).

The monkey was placed into a MRI-compatible stereotactic apparatus (Kopf, Inc.). Local anesthetic (lidocaine cream) was applied to the ends of the ear bars and ophthalmic ointment was applied to the eyelids to minimize discomfort induced by the stereotactic apparatus. A heating pad was placed beneath the monkey to maintain a constant body temperature.

MRI-Compatible Reversible Deactivation (RD) of the Cortex Using a Cooling System

A small portion of the primary visual cortex of the right hemisphere was deactivated by placing an MRI-compatible coolant probe on the surface of the dura above V1. The probe was made from G10/FR4 (fiberglass). Up to three MRI-compatible fiber optic thermocouples (00-11874-01, Luxtron Corp.) were placed on the lateral side of the probe (see Fig. 1) surrounding the cooling surface. During the experiments on the second monkey, the recording well was adapted to allow a thermocouple to be placed directly under the cryo-surface of the cooling probe. All thermocouples touched the dura during the experiment and yielded a real time measure of the cortical surface temperature either immediately below or lateral to the cooling probe. Methanol (reagent grade anhydrogenous, S75965, Fisher Scientific) was passed through the probe with a pump (QV pump, Q3 pump head, FMI Pump). Teflon tubing (1667xl,

Upchurch Scientific) was used to transfer the methanol from the pump, and ferrules and nuts (P-343 ferrule, P-331 nut, Upchurch Scientific) were used to secure the tubing to the pump and coolant probe. An illustration of the MRI-compatible cooling probe and a schematic of the placement of the probe relative to the brain are shown in Figure 1.

MR-Based Thermometry

MR thermometry imaging used single shot multi-slice echo planar imaging with an isotropic resolution of 2.0 mm. Twenty-five axial slices were acquired using repetition time/echo time (TR/TE) = 4000/19 ms, 128 mm field of view, and a 90° flip angle. Magnitude and phase images were acquired.

Temperature maps were calculated from the MR thermometry scans using the proton resonance frequency shift thermometry (PRFST) method which relates the temperature change to the difference in phase between successive time points (22,23). The equation reads:

$$\Delta\varphi = 2\pi \cdot \alpha \cdot \omega \cdot \mathrm{TE} \cdot \Delta T \quad [1]$$

where $\Delta\varphi$ is the change in phase, α is the thermal coefficient (0.01 ppm/°C), ω is the resonance frequency, TE is the echo time of the pulse sequence, and ΔT is the temperature change. Equation [1] needed to be modified to account for the linear phase drift which occurs even in voxels where the temperature does not change. The phase drift is caused by heating of the gradient and shim coils during heavy duty cycles. The change in the phase drift is constant over the image so Eq. (1) can be rewritten as:

$$\Delta\varphi = 2\pi \cdot \alpha \cdot \omega \cdot \mathrm{TE} \cdot \Delta T + \Delta\varphi_{\mathrm{drift}} \quad [2]$$

where $\Delta\varphi_{\mathrm{drift}}$ is calculated in a region far from the probe (i.e., the left frontal lobe) where the temperature has not changed.

Quantification of Accuracy and Precision of Ex Vivo MR Thermometry

The accuracy and precision of the MR temperature maps was quantified by cooling ex vivo bovine muscle tissue. One cooling cycle lasted 5.5 min and was followed by a warm epoch of 7 min. The accuracy of the MR temperature maps relative to the thermocouple readings was quantified by averaging four voxels surrounding the thermocouple. The precision of the MR temperature maps was quantified by calculating the standard deviation of the temperature in a region far from the cooling probe. The location of the thermocouple could be accurately (2 mm) determined by locating sharp changes in the phase maps.

Temperature maps were calculated using Eq. (2). Figure 2a shows a 2-dimensional temperature map of a slice (at a $2.1 \times 2.1 \times 1$ mm^3 spatial resolution) under the cooling probe. Figure 2b shows the MR thermometry values (averaged from four voxels in the first slice under the probe) as compared to the thermocouple measurements from the same location.

The precision of the MR-based temperature maps was ± 1.8°C and the accuracy of the average of four voxels was within ± 0.7°C of the thermocouple measurements. The high correlation coefficient between the MR thermometry maps and the thermocouple ($r^2 = 0.99$) indicates the robustness of the phase difference method for calculating temperature.

Measurement of the ADC and FA During In Vivo Reversible Deactivation of Cerebral Metabolism

Experimental Design—DTI was acquired at the beginning of the experiment while room temperature (23°C) methanol flowed through the coolant probe (~ 12 min). The brain was then cooled for 11 min while MR-based thermometry images were taken. Flow rates ranged from 50 mL/min–120 mL/min and inlet temperatures of the methanol (1 meter from probe) ranged from −30°C to −70°C during the experiments. Only methanol flow rates > 80 mL/min and inlet methanol temperatures < −40°C resulted in cortical temperatures of < 20°C, the threshold temperature at which cortical metabolism is blocked (17). Such low inlet temperatures were needed because of the thermal conductivity properties of the fiberglass used to build the cooling probe. After 11 min, the temperature distribution in the brain was at equilibrium as measured by the PRFST method and the stability of the supra-dural thermocouple readings. DTI was acquired during the remainder of the cooling period (~ 30 min). The temperature of the brain was then raised for 8 min using methanol at room temperature while MR thermometry images were taken. DTI images were then taken during the recovery period. Below follows a description of the DTI, MR thermometry, and T1-weighted images acquired.

DTI—Twenty-five axial slices were taken of the monkey at a slice thickness of 2.0 mm (with 0 mm skip). The in-plane resolution was 2.0 × 2.0 mm, with a matrix size of 64 × 64. The sequence parameters were TR/TE = 5500/87 ms, b = 700 s mm^{-2}. The diffusion gradient sampling scheme consisted of n = 60 directions which were obtained using the electrostatic shell method (27). Ten images with no diffusion-weighting were also obtained for a total of 70 acquisitions. The total acquisition time was 5 min 31 sec. ADC and FA maps were calculated from the log signal relation using the b = 0 and b = 700 s/mm^2 scan (28). Because the temperature was held constant during the diffusion scans, the relaxation rate was a constant between the b = 0 and diffusion weighted scans (b = 700 s/mm^2).

Low-Resolution T1 Images—Low-resolution T1 images were acquired during each trial with an MPRAGE sequence (29) with TR/TI/TE = 2730/ 1100/3.19 ms, α = 8°, 1.5 mm isotropic resolution, total acquisition time: 2 min 54 s.

Six T1 images were acquired for all experiments with this sequence and reconstructed (motion corrected, averaged and normalized) using Freesurfer, http://surfer.nmr.mgh.harvard.edu (30). All diffusion and temperature maps from an individual trial were registered to this image. The low-resolution T1 image was then registered to the high resolution image (template). The transformation matrix from this registration was then applied to the diffusion and temperature maps so all analysis could be performed in the high resolution coordinates.

High-Resolution T1 Images—For both monkeys, high resolution T1 images were acquired in a separate session with an MPRAGE sequence (29) with TR/TI/TE = 2500/1100/4 ms, α = 8°, 0.35 mm isotropic resolution, total acquisition time: 16 min. Eight T1 images were acquired with this sequence and reconstructed (motion corrected, averaged, and normalized) using Freesurfer, http://surfer.nmr.mgh.harvard.edu. The resulting T1 image was used as a template to co-register all diffusion images, and temperature maps.

Thermocouple Measurements—Using a Luxtron 3100 Fluoroptic Thermometer (Luxtron Corp.), thermocouple readings were stored at a rate of 4 Hz. The thermocouple readings were used during the experiment to approximate the temperature of the deactivated region and to ensure an equilibrium temperature distribution during the cooling period (as was always verified post hoc using the PRFST method).

Image Registration and Visualization—Images were registered using the flirt command (rigid registration, 6 degrees of freedom) in the FSL toolbox (http://www.fmrib.ox.ac.uk). All visualization postprocessing was performed using custom software written in Matlab (version 6.5.1.199709 (R13) Service Pack 1).

Statistical Analysis

Nonparametric permutation testing (NPPT) was applied using the method of Nichols (31). For each experiment, n = 500 permutations of 5 time points of the warm condition and 5 time points of the cold condition were performed. *P*-value maps were generated using a standard two tailed t-test. The maximum cluster size was calculated for each permutation considering *P*-values < 0.05 using Matlab with a connectivity of 26 (i.e., each voxel in the cluster was surrounded by 26 statistically significant voxels, $P < 0.05$). The final *P*-value map was calculated using the equation:

$$P_{final} = \frac{\sum_{n=1}^{500} (P_i < P_o)}{n} \quad [3]$$

where p_o is the *P* value of the original time series and p_i is the *P*-value from the i^{th} random permutation of the time series. The threshold for the size of statistically significant regions in the final *P*-value map was determined by considering the distribution of the maximum cluster size. The minimum statistically significant cluster size was determined to be the 25th largest cluster size in the maximum cluster size distribution (i.e., 5% confidence for n = 500 is 25). The results from the NPPT analysis were used to determine suitable regions for the region of interest (ROI) analysis (see below).

ROI Analysis

The regions showing a statistically significant change in ADC as determined by the NPPT analysis was split into three sub ROIs based on the temperature distribution during the cold epochs. The three temperature ranges were: 34–40°C (no temperature change), 20–34°C (cooled, although not completely deactivated region), 8–20°C (completely deactivated region). The value of 34°C was chosen as the normal background temperature of the brain because the precision of the ex vivo temperature measurements in a voxel was ±1.0°C at a resolution of 2.0 × 2.0 × 2.0 mm. Thus, 37 ± 3σ or 37 ± 3°C represented the 99% confidence interval where temperature did not change significantly ($P > 0.01$) from the normal brain temperature.

RESULTS

In Vivo Reversible Deactivation Experiment

Diffusion tensor imaging (DTI) was acquired during a warm or “normal temperature” epoch (12 min) while warm (20°C) methanol was pumped through the cooling probe. This ensured that potential changes in diffusion as measured during the cold epochs could not be merely attributed to changes in methanol flow. Thereafter, we cooled a portion of the primary visual cortex (right hemisphere, lower visual field, 0.7 cm^2 surface) and acquired MR temperature maps until the temperature, as measured by the supra-dural MRI-compatible thermocouple positioned immediately beneath the cooling probe (or lateral to the probe), reached the desired steady state temperature. By altering the flow rate of the methanol during each experiment, we were able to reach a steady-state cortical temperature (~ 30 min duration) immediately below the cooling probe of, T_c = 37, 34, 29, 26, 22, 11 (cortical deactivation experiment #1, M1), 9.5 (cortical deactivation experiment #1, M2), 8°C (cortical deactivation experiment #2, M1), 8°

C (cortical deactivation experiment #1, M3). During the experiment at 22°C the cortex was near but still above the metabolic cutoff temperature. During the experiments where the cortex reached a temperature of respectively 11, 9.5, and 8°C (M1, M3) the brain was cooled as low as possible with-out inflicting damage to the dura. During the remainder of the cooling period we kept the cortical temperature constant while DTI images were acquired. Finally, the brain temperature was allowed to recover by pumping through warm ethanol (20°C), while MR temperature maps were acquired (~ 8 min). When the thermocouples revealed a steady-state "recovered" temperature of 30°C, we acquired three additional DTI images.

ADC Decrease During Metabolic Deactivation

Figure 3 shows examples of the raw ADC (top row) and FA maps (bottom row) acquired during the (1) warm, (2) cold, and (3) recovery conditions of cortical deactivation experiment #2 (M1). Note the difference in ADC maps during the cold condition in the region under the probe when the temperature was 8°C (white rectangle). No such change is obvious in the FA maps (bottom row, Fig. 3).

To identify voxels showing a significant change ($P < 0.05$) in ADC and FA between the warm and cooling epochs, we used non parametric permutation testing (NPPT, see the Methods section) (31).

Nonparametric Permutation Testing (NPPT)

The entire brain volume was used for the NPPT analyses (both for the ADC and the FA maps). Importantly, the NPPT analyses revealed cooling-induced ADC changes only in those experiments where cortical tissue was cooled well below 20°C—thus not even in the experiment in which the cortical temperature reached 22°C. Figure 4a,b shows large brain regions in M1 (3.36 cm^3 brain tissue) and M2 (3.83 cm^3) where the ADC had decreased significantly ($P < 0.05$) when $T_c = 11$°C (cortical deactivation #1, M1). Those results suggest already that ADC changes depend on processes directly dependent on metabolism (which is silenced < 20°C) and not on temperature alone.

To answer the question whether the observed ADC changes were restricted to these voxels in which the temperature was below 20°C (i.e., the cortex where metabolic activity was blocked) or whether the ADC changes extended outside the deactivated region, we calculated the 3D temperature maps using the PRFST method and overlaid them upon the ADC maps. The 20°C isothermal reveals the region of the cortex where metabolism has been completely blocked (17,19). Figure 4 shows decreased ADC in regions where the temperature did not change (> 34°C). The amplitude of the observed ADC changes in the region where temperature did not change was similar across all three monkeys (see Table 1), although the effect was spatially more extended in M1 and M3 compared with M2 (40% of the region calculated from NPPT in M1, 75% in M3, and 10% in M2).

The ADC changes at a distance from the cooling probe were most apparent in M3. Figure 5 shows the region where the ADC changed (in red) compared with the temperature maps. Changes in the ADC are seen far from the cooling probe despite the fact that the deactivation region was very restricted.

ROI Analysis

To quantify the ADC changes as a function of temperature, we performed a ROI analysis for the three experiments in which the cortex was cooled below the critical temperature of 20°C (i.e., to 11°C, 9.5°C, or 8°C). To restrict our analysis to gray or white matter voxels, we masked the voxels corresponding to cerebral spinal fluid (CSF) from the ADC maps at a threshold of

ADC < 0.0012 mm^2/s. It was determined that only 7% of all the voxels showing a decrease in ADC in M1, 3% in M2, and 6% in M3 were CSF.

We defined three ROIs (ROI 1–3) which were based on the isothermals as measured during the cold epochs. Those three ROIs encompassed voxels that showed a significant change in ADC as defined by the NPPT analysis, and they were further subdivided in gray and white matter compartments. ROI 1 included those voxels that did *not* change in temperature during the cold epochs (34–40°C) and ROI 2 and 3 showed significant ADC changes when the temperature during the cooling period was between 20–34°C, or between 8 and 20°C, respectively.

Table 1 shows the normalized ADC values from ROIs 1–3 during the warm, cold, and recovery conditions. The data were normalized to the first warm ADC value. Unlike the ADC changes observed during the cold epoch in ROI 1, the ADC changes in ROIs 2 and 3 could be (partially) due to temperature changes. Below, we will argue that temperature is most likely not the only factor contributing to the observed ADC decrease in the voxels < 34°C. Note that, despite the very cold inlet methanol, we were able to cool cortex below the metabolic cutoff temperature of 20°C only in a relatively small region (0.2 cm^3 voxels in M1 and 0.4 cm^3 in M2).

We assume that the temperature distribution throughout the brain remains constant throughout the 30 min that DTI images are acquired. We believe that this is the case because the thermocouple measurements at the cortical surface remained constant throughout the cooling period. Second, the temporal characteristics of the ADC measurements showed that they were stable throughout the same cooling period. Indeed, Figure 6 shows the mean normalized ADC (± SEM) in M1 versus time in three temperature ranges: 8–20°C (ROI 3), 20–34°C (ROI 2), 34–40°C (ROI 1). The ADC values were constant during the cold conditions in each ROI, which indicates the brain was already deactivated at the beginning of the cold condition and the temperature inside the brain had reached equilibrium when we started the acquisition of these DTI images.

In Vivo ADC as a Function of Temperature

The previous analysis revealed that in a substantial fraction of voxels, in which the temperature did not change, the ADC values decreased. Moreover, these changes were only observed in those experiments where at least a small fraction of the cortex was cooled below 20°C. Hence, only those experiments where metabolism could be completely blocked resulted in decreased ADC values. Furthermore, if ADC is dependent on “normal” metabolism, one would expect that ADC decreases in “cold” voxels (< 20°C) are larger than that predicted by temperature alone. Using the data from the nine reversible deactivation experiments, we tested this hypothesis by calculating the in vivo ADC as a function of temperature and compared it with the diffusion of free water (32,33). The voxels of ROI 1, that could be completely deactivated in 3/9 experiments (i.e., ROI 1, T < 20°C), were used to calculate the ADC as a function of temperature for all 10 experiments (the same voxels reached a different temperature in each one of those 10 experiments). Figure 7 plots the in vivo ADC as a function of temperature relative the diffusion of free water. The in vivo ADC follows the same trend as the diffusion of free water above the metabolic cutoff (on the right of the vertical dotted line) but shows a significant decrease relative to the diffusion of free water only below the metabolic cutoff (data points on the left of the black dotted line). This result suggests that a substantial fraction of the ADC depends on processes directly dependent on metabolism and not on temperature alone. Table 2 presents the difference between normalized $ADC_{\text{in vivo}} - ADC_{\text{free water}}$. The normalized ADC of free water was interpolated to the temperature points of the 9 reversible deactivation experiments with a second order polynomial. Statistically significant decreases in the $ADC_{\text{in vivo}}$ relative to that of free water were only observed below the metabolic cutoff and

ranged between 22–25%. It is likely that the ADC decrease in the deactivation region was underestimated because of an increase in blood flow to compensate cooling.

FA Shows No Change During Metabolic Deactivation

Using the same NPPT analysis as for the ADC data, we compared the FA maps between all combinations of the warm, cold, and recovery conditions. In addition, we compared the FA values in ROI 1, 2, and 3 between the warm, cold, and recovery conditions. None of these analyses revealed changes in the FA maps during cortical cooling, in either monkey.

DISCUSSION

Effect of Cerebral Metabolism on the ADC and FA

Reversible deactivation of cerebral metabolism by cortical cooling resulted in ADC decreases of 12–21% in regions far from the cooling probe, in voxels where the temperature did not change (Fig. 4, Fig. 5). No changes in FA could be revealed using NPPT analysis, nor using more sensitive ROI-based statistics. The decrease in ADC at distant sites induced by cooling can be explained by the effect that cooling has on processes regulated by cerebral metabolism. Cooling reduces deoxyglucose uptake in neurons that are at a temperature below 20°C (21, 34,35). Moreover, cortical cooling has a profound functional effect at distant sites receiving anatomical projections from the deactivated region (21,36). In addition, reversible deactivation studies using cooling in combination with electrophysiology indicated that action potentials cannot be generated below 20°C, hence cooling also blocks neuronal activity (17).

In the present study, changes in ADC were revealed *only* during those cooling experiments where the cortical temperature under the cooling probe was below the metabolic cutoff of 20° C and not in those experiments where the cortical temperature was > 20°C. This strongly indicates that the ADC depends on metabolism. This is also supported by the marked decrease of the in vivo ADC (22–25%) compared with that of free water below the metabolic cutoff of 20°C. The magnitude of this decrease agrees with the ADC decrease in regions where the temperature did not change. It is tempting to suggest that those regions showing an ADC decrease but no change in temperature are anatomically connected to the region which was effectively deactivated. These results indicate that the changes in ADC are not due to the effect of temperature on diffusion alone and are due to the deactivation of cerebral metabolism in a small portion of the cortex.

Which biophysical mechanism that depends on cerebral metabolism could be responsible for such ADC changes? One possible mechanism could be fast axonal transport (cytosolic streaming) (10). Fast axonal transport of proteins and vesicles is induced by the motion of the microfilaments and microtubuli (37) and is regulated by ATP (38). Local anoxia (cold-block) experiments showed inhibition of fast axonal transport by affecting oxidative metabolism responsible for ATP production (39–42). It is possible that the reversible deactivation of cerebral metabolism by cooling affected the diffusion of water by inhibiting the fast axonal transport throughout the axon. The diffusion coefficient of water arising from fast axonal transport can be calculated by assuming a parabolic velocity profile of water in the axon with no flow on the boundary of the axon and a maximum velocity, v_{max}, in the center of the axon. The range of v_{max} can be approximated by the velocity range of the fast axonal transport of proteins, v_{max} = 1–10 μm/s (43–46). The range of diffusion coefficients resulting from this parabolic flow profile would be $2.5 < D < 250$ μm^2/ms which is partially in the range of diffusion coefficients, $D \cong 0.1 – 10$ μm^2/ms, as measured in the brain.

Another possible mechanism which could explain the ADC decrease at distant sites from cooling is neuronal activity. As local deactivation of cerebral metabolism has been shown to

affect action potential generation at distant sites (21), changes in the electric potential of axons and neurons can affect the diffusion of water (47). When the cell is active, the electrical potential and phenomena directly related to action potential generation (e.g., the displacement of water associated with the flow of ions through ion channels or pumps) may act as a driving force for the diffusion of water and other materials (proteins, vesicles) along the axon.

ADC decreases observed during this experiment (12–21%) could partially explain the marked decrease in ADC during ischemia (in which cerebral metabolism is affected) of 20–50% (48, 49) and postmortem studies (~ 40%) (9). FA changes were not expected to change because of the short deactivation period (~ 30 min). FA changes in stroke and lesion studies have been shown to occur over a long time period (hours to days) and may be related to neural processes like Wallerian degeneration (14) and other changes to the neuroarchitecture.

Although the results in this study may compel one to deduce that the ADC in the brain has a metabolic component, the limited sample size in this experiment prevents this conclusion. Future studies with large populations of rats would provide the necessary biostatistics to justify such a statement. To provide conclusive evidence of a link between ADC and metabolism, other reversible deactivation techniques also may be used. Besides cortical cooling, reversible deactivations can be achieved using pharmacological approaches (e.g., injection of local anesthetics and GABA agonists, fast axonal transport and action potential blockers (47), etc.). Drug-induced deactivations, however, have two disadvantages, (a) a limited number of drug injections can be performed before the cortical tissue is severely damaged, and (b) it is more difficult to quantify the deactivation region because of the low MR sensitivity (10^{-5}) of NMR spectroscopy compared with conventional MRI. In the present experiments, cortical cooling was chosen because it allowed focal deactivation of cerebral metabolism over a shorter time scale (~ min) as compared to drug injection (~ hours) (20). Hence, we could perform multiple deactivations during the same scan session. However, reversible deactivation in conjunction with MR-spectroscopy could measure which metabolites are suppressed during deactivation to more accurately quantify the effects of cooling on cerebral metabolism.

It would also be of great interest to study the blood flow during cortical cooling reversible deactivation to understand the physiological response of the brain to metabolic changes. These studies could address if blood flow is increasing to the deactivated region and address how local can the temperature (and thus deactivation) control be. Although the authors believe that the small volume fraction of blood could not cause the magnitude of the diffusion changes measured in this experiment, it is possible that maybe there is increase/decrease in blood flow, thus, mitigating the diffusion effect.

Future Work

The results from this experiment validate the methodology developed to reversible deactivate cerebral metabolism in the brain and perform MRI measurements. In a latter study, the diffusion MRI results during reversible deactivation will be compared the hemodynamic response throughout visual cortex to determine the relationship between water diffusion and the hemodynamic response. The MRI-compatible cortical cooling system presented in this study will also be used to explore functional interactions between anatomically connected regions (50). The fast deactivation capabilities of the cooling system (~ 4 min) makes it ideal for fMRI studies (51–53) in which regions can be deactivated and re-activated many times within a typical scan session.

Finally, the results from this experiment suggests that futures studies which explore the relationship between cerebral metabolism, anoxic depolarization, cell volume, and acute ADC changes would provide valuable information regarding the underlying biophysical mechanisms of the diffusion MRI signal (54–57).

CONCLUSION

In summary, we presented a novel in vivo method to deactivate cerebral metabolism in an MRI-compatible, focal, and reversible manner. Combined with in vivo 3D thermometry measurements with an accuracy of ±1°C, the present experiments indicated that reversible short-term deactivation of the cortex resulted in a significant decrease in the ADC at distant sites from cooling but has no measurable effect on FA. In our study, we used MR temperature maps to show that ADC decreases (12–21%) occurred even in restricted locations where the temperature did not change. Furthermore, the temperature dependence of in vivo ADC follows that of free water above the metabolic cutoff of 20°C but shows a marked deviation (i.e., a 22–25% decrease) below the metabolic cutoff. These data suggest that a relatively large fraction of ADC in V1 in the monkey brain depends on normal metabolism. By using the technology developed in this study to examine the hemodynamic response, we can understand the relationship between the hemodynamic response and water diffusion.

Acknowledgments

The authors thank Thomas Benner, Ken Kwong, Giorgio Bonmasser, Larry Wald, Leonardo Angelone, Andreas Potthast, and Helen Deng for their assistance with this project, and Sow Hsin-Chen of the Nuclear Science and Engineering Department at MIT for his helpful discussions on the hydrodynamics of proteins. This work was supported by 5R01EB00790-04, IUAP 5/04, EF/05/014, FWO G151.04, HFSPO RGY0014/2002-C, GSKE, NINDS NS46532, NCRR RR14075, NCI CA09502, NCI 5T32CA09502, GlaxoSmith-Kline, the Athinoula A. Martinos Foundation, the Mental Illness and Neuroscience Discovery (MIND) Institute, and the National Alliance for Medical Image Computing (NAMIC) (NIBIB EB05149) which is funded through the NIH Roadmap for Medical Research.

REFERENCES

1. Callaghan, P. Principles of nuclear magnetic resonance microscopy. Oxford: Oxford Press; 1993.
2. Okubo T, Aoki S, Abe O, Masutani Y, Ohtomo K, Hori M, Ishigame K, Araki T. [Principles of diffusion-weighted MR imaging and application to clinical neurology]. Rinsho Shinkeigaku 2004;44:954–956. [PubMed: 15651342]
3. Rosenbloom M, Sullivan EV, Pfefferbaum A. Using magnetic resonance imaging and diffusion tensor imaging to assess brain damage in alcoholics. Alcohol Res Health 2003;27:146–152. [PubMed: 15303625]
4. Basser PJ, Pajevic S, Pierpaoli C, Duda J, Aldroubi A. In vivo fiber tractography using DT-MRI data. Magn Reson Med 2000;44:625–632. [PubMed: 11025519]
5. Catani M, Howard RJ, Pajevic S, Jones DK. Virtual in vivo interactive dissection of white matter fasciculi in the human brain. Neuroimage 2002;17:77–94. [PubMed: 12482069]
6. Parker GJ, Stephan KE, Barker GJ, Rowe JB, MacManus DG, Wheeler-Kingshott CA, Ciccarelli O, Passingham RE, Spinks RL, Lemon RN, Turner R. Initial demonstration of in vivo tracing of axonal projections in the macaque brain and comparison with the human brain using diffusion tensor imaging and fast marching tractography. Neuroimage 2002;15:797–809. [PubMed: 11906221]
7. Wakana S, Jiang H, Nagae-Poetscher LM, van Zijl PC, Mori S. Fiber tract-based atlas of human white matter anatomy. Radiology 2004;230:77–87. [PubMed: 14645885]
8. Le Bihan D, Urayama S, Aso T, Hanakawa T, Fukuyama H. Direct and fast detection of neuronal activation in the human brain with diffusion MRI. Proc Natl Acad Sci U S A 2006;103:8263–8268. [PubMed: 16702549]
9. Beaulieu C. The basis of anisotropic water diffusion in the nervous system - a technical review. NMR Biomed 2002;15:435–455. [PubMed: 12489094]
10. Beaulieu C, Allen PS. Determinants of anisotropic water diffusion in nerves. Magn Reson Med 1994;31:394–400. [PubMed: 8208115]
11. Partridge SC, Mukherjee P, Henry RG, Miller SP, Berman JI, Jin H, Lu Y, Glenn OA, Ferriero DM, Barkovich AJ, Vigneron DB. Diffusion tensor imaging: serial quantitation of white matter tract maturity in premature newborns. Neuroimage 2004;22:1302–1314. [PubMed: 15219602]

12. Elshafiey I, Bilgen M, He R, Narayana PA. In vivo diffusion tensor imaging of rat spinal cord at 7 T. Magn Reson Imaging 2002;20:243–247. [PubMed: 12117606]
13. Mukherjee P, Miller JH, Shimony JS, Conturo TE, Lee BC, Almli CR, McKinstry RC. Normal brain maturation during childhood: developmental trends characterized with diffusion-tensor MR imaging. Radiology 2001;221:349–358. [PubMed: 11687675]
14. Pierpaoli C, Barnett A, Pajevic S, Chen R, Penix LR, Virta A, Basser P. Water diffusion changes in Wallerian degeneration and their dependence on white matter architecture. Neuroimage 2001;13(Pt 1):1174–1185. [PubMed: 11352623]
15. Watanabe T, Honda Y, Fujii Y, Koyama M, Tanaka R. Serial evaluation of axonal function in patients with brain death by using anisotropic diffusion-weighted magnetic resonance imaging. J Neurosurg 2004;100:56–60. [PubMed: 14743912]
16. Sehy JV, Zhao L, Xu J, Rayala HJ, Ackerman JJ, Neil JJ. Effects of physiologic challenge on the ADC of intracellular water in the Xenopus oocyte. Magn Reson Med 2004;52:239–247. [PubMed: 15282805]
17. Lomber SG, Payne BR, Horel JA. The cryoloop: an adaptable reversible cooling deactivation method for behavioral or electrophysiological assessment of neural function. J Neurosci Methods 1999;86:179–194. [PubMed: 10065985]
18. Lomber SG. The advantages and limitations of permanent or reversible deactivation techniques in the assessment of neural function. J Neurosci Methods 1999;86:109–117. [PubMed: 10065980]
19. Lomber SG, Payne BR. Translaminar differentiation of visually guided behaviors revealed by restricted cerebral cooling deactivation. Cereb Cortex 2000;10:1066–1077. [PubMed: 11053228]
20. Lomber, SG. Virtual lesions. Oxford: Oxford Press; 2002.
21. Vanduffel W, Payne BR, Lomber SG, Orban GA. Functional impact of cerebral connections. Proc Natl Acad Sci U S A 1997;94:7617–7620. [PubMed: 9207141]
22. De Poorter J, De Wagter C, De Deene Y, Thomsen C, Stahlberg F, Achten E. Noninvasive MRI thermometry with the proton resonance frequency (PRF) method: in vivo results in human muscle. Magn Reson Med 1995;33:74–81. [PubMed: 7891538]
23. MacFall JR, Prescott DM, Charles HC, Samulski TV. 1H MRI phase thermometry in vivo in canine brain, muscle, and tumor tissue. Med Phys 1996;23:1775–1782. [PubMed: 8946373]
24. Turner R, Le Bihan D, Maier J, Vavrek R, Hedges LK, Pekar J. Echo-planar imaging of intravoxel incoherent motion. Radiology 1990;177:407–414. [PubMed: 2217777]
25. Leenders KL, Perani D, Lammertsma AA, Heather JD, Buckingham P, Healy MJ, Gibbs JM, Wise RJ, Hatazawa J, Herold S. Cerebral blood flow, blood volume and oxygen utilization. Normal values and effect of age. Brain 1990;113(Pt 1):27–47. [PubMed: 2302536]
26. Rostrup E, Knudsen GM, Law I, Holm S, Larsson HB, Paulson OB. The relationship between cerebral blood flow and volume in humans. Neuroimage 2005;24:1–11. [PubMed: 15588591]
27. Jones DK, Horsfield MA, Simmons A. Optimal strategies for measuring diffusion in anisotropic systems by magnetic resonance imaging. Magn Reson Med 1999;42:515–525. [PubMed: 10467296]
28. Basser PJ, Mattiello J, LeBihan D. MR diffusion tensor spectroscopy and imagings. Biophys J 1994;66:259–267. [PubMed: 8130344]
29. Mugler JP III, Brookeman JR. Three-dimensional magnetization-prepared rapid gradient-echo imaging (3D MP RAGE). Magn Reson Med 1990;15:152–157. [PubMed: 2374495]
30. Dale AM, Fischl B, Sereno MI. Cortical surface-based analysis. I. Segmentation and surface reconstruction. Neuroimage 1999;9:179–194. [PubMed: 9931268]
31. Nichols TE, Holmes AP. Nonparametric permutation tests for functional neuroimaging: a primer with examples. Hum Brain Mapp 2002;15:1–25. [PubMed: 11747097]
32. Mills R. Self-diffusion in normal and heavy water in the range 1–45 C. J Phys Chem 1973;77:685–688.
33. Thelwall PE, Shepherd TM, Stanisz GJ, Blackband SJ. Effects of temperature and aldehyde fixation on tissue water diffusion properties, studied in an erythrocyte ghost tissue model. Magn Reson Med 2006;56:282–289. [PubMed: 16841346]

34. Sokoloff L. The deoxyglucose method for the measurement of local glucose utilization and the mapping of local functional activity in the central nervous system. Int Rev Neurobiol 1981;22:287–333. [PubMed: 7024169]
35. Sokoloff L, Reivich M, Kennedy C, Des Rosiers MH, Patlak CS, Pettigrew KD, Sakurada O, Shinohara M. The [14C]deoxyglucose method for the measurement of local cerebral glucose utilization: theory, procedure, and normal values in the conscious and anesthetized albino rat. J Neurochem 1977;28:897–916. [PubMed: 864466]
36. Vanduffel W, Orban GA, Lomber SG, Payne BR. Functional impact of cerebral projection systems. Mol Psychiatry 1998;3:215–219. [PubMed: 9672896]
37. Hammerschlag, R.; Brady, S. Axonal transport and the neuronal cytoskeleton. In: Siegel, G.; Agranoff, B.; Albers, W.; Molinoff, P., editors. Basic neurochemistry. New York: Raven Press; 1989. p. 457-478.
38. Ochs S. Trophic functions of the neuron. 3. Mechanisms of neurotrophic interactions. Systems of material transport in nerve fibers (axoplasmic transport) related to nerve function and trophic control. Ann N Y Acad Sci 1974;228:202–223. [PubMed: 4135388]
39. Ochs S. Local supply of energy to the fast axoplasmic transport mechanism. Proc Natl Acad Sci U S A 1971;68:1279–1282. [PubMed: 5288375]
40. Ochs S. Fast transport of materials in mammalian nerve fibers. Science 1972;176:252–260. [PubMed: 5019778]
41. Ochs S, Sabri MI, Johnson J. Fast transport system of materials in mammalian nerve fibers. Science 1969;163:686–687. [PubMed: 5762934]
42. Smith RS, Snyder RE. Anterograde to retrograde reversal of fast axonal transport within cold blocked and rewarmed intact axons. Brain Res 1995;672:205–213. [PubMed: 7749742]
43. Brimijoin S. Stop-flow: a new technique for measuring axonal transport, and its application to the transport of dopamine-beta-hydroxylase. J Neurobiol 1975;6:379–394. [PubMed: 52690]
44. Oaklander AL, Spencer PS. Cold blockade of axonal transport activates premitotic activity of Schwann cells and wallerian degeneration. J Neurochem 1988;50:490–496. [PubMed: 2447241]
45. Koike H. The disturbance of the fast axonal transport of protein by passive stretching of an axon in Aplysia. J Physiol 1987;390:489–500. [PubMed: 2450998]
46. Koike H, Matsumoto H. Fast axonal transport of membrane protein and intra-axonal diffusion of free leucine in a neuron of Aplysia. Neurosci Res 1985;2:281–285. [PubMed: 2410835]
47. de Crespigny A, Rother J, van Bruggen N, Beaulieu C, Moseley ME. Magnetic resonance imaging assessment of cerebral hemodynamics during spreading depression in rats. J Cereb Blood Flow Metab 1998;18:1008–1017. [PubMed: 9740104]
48. Moseley ME, Kucharczyk J, Mintorovitch J, Cohen Y, Kurhanewicz J, Derugin N, Asgari H, Norman D. Diffusion-weighted MR imaging of acute stroke: correlation with T2-weighted and magnetic susceptibility-enhanced MR imaging in cats. AJNR Am J Neuroradiol 1990;11:423–429. [PubMed: 2161612]
49. Turner R, Le Bihan D, Maier J, Vavrek R, Hedges LK, Pekar J. Echo-planar imaging of intravoxel incoherent motion. Radiology 1990;177:407–414. [PubMed: 2217777]
50. Khachaturian, MH.; Arsenault, JT.; Ekstrom, LB.; Vanduffel, W. Reversible deactivation of area V1 modulates visually-driven activity in several visual structures: an awake monkey fMRI study. Proceedings of the 37th Annual Meeting of SfN; San Diego, California, USA. 2007.
51. Vanduffel W, Fize D, Mandeville JB, Nelissen K, Van Hecke P, Rosen BR, Tootell RB, Orban GA. Visual motion processing investigated using contrast agent-enhanced fMRI in awake behaving monkeys. Neuron 2001;32:565–577. [PubMed: 11719199]
52. Nelissen K, Vanduffel W, Orban GA. Charting the lower superior temporal region, a new motion-sensitive region in monkey superior temporal sulcus. J Neurosci 2006;26:5929–5947. [PubMed: 16738235]
53. Sasaki Y, Rajimehr R, Kim BW, Ekstrom LB, Vanduffel W, Tootell RB. The radial bias: a different slant on visual orientation sensitivity in human and nonhuman primates. Neuron 2006;51:661–670. [PubMed: 16950163]
54. King MD, Crowder MJ, Hand DJ, Harris NG, Williams SR, Obrenovitch TP, Gadian DG. Temporal relation between the ADC and DC potential responses to transient focal ischemia in the rat: a Markov

chain Monte Carlo simulation analysis. J Cereb Blood Flow Metab 2003;23:677–688. [PubMed: 12796716]

55. Harris NG, Zilkha E, Houseman J, Symms MR, Obrenovitch TP, Williams SR. The relationship between the apparent diffusion coefficient measured by magnetic resonance imaging, anoxic depolarization, and glutamate efflux during experimental cerebral ischemia. J Cereb Blood Flow Metab 2000;20:28–36. [PubMed: 10616790]
56. de Crespigny AJ, Rother J, Beaulieu C, Moseley ME, Hoehn M. Rapid monitoring of diffusion, DC potential, and blood oxygenation changes during global ischemia. Effects of hypoglycemia, hyperglycemia, and TTX. Stroke 1999;30:2212–2222. [PubMed: 10512931]
57. Verheul HB, Balazs R, Berkelbach van der Sprenkel JW, Tulleken CA, Nicolay K, Tamminga KS, van Lookeren Campagne M. Comparison of diffusion-weighted MRI with changes in cell volume in a rat model of brain injury. NMR Biomed 1994;7:96–100. [PubMed: 8068532]

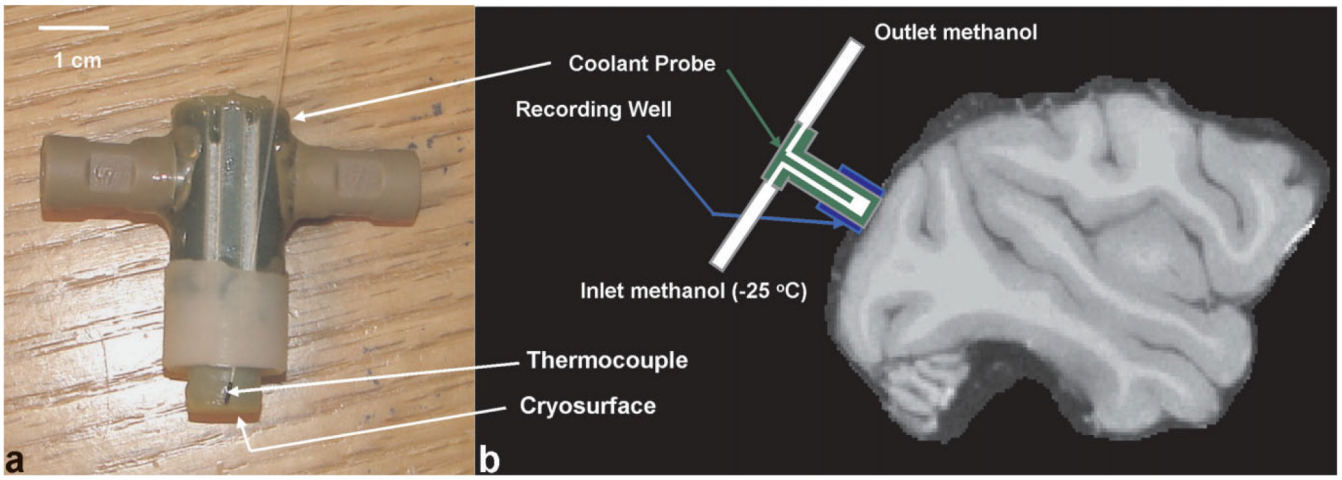

FIG. 1.

a: Coolant probe used and attached thermocouples. **b:** Schematic (not to scale) of coolant probe orientation on the dura above V1. The radial symmetry of the probe ensured that it was in the same position for each experiment.

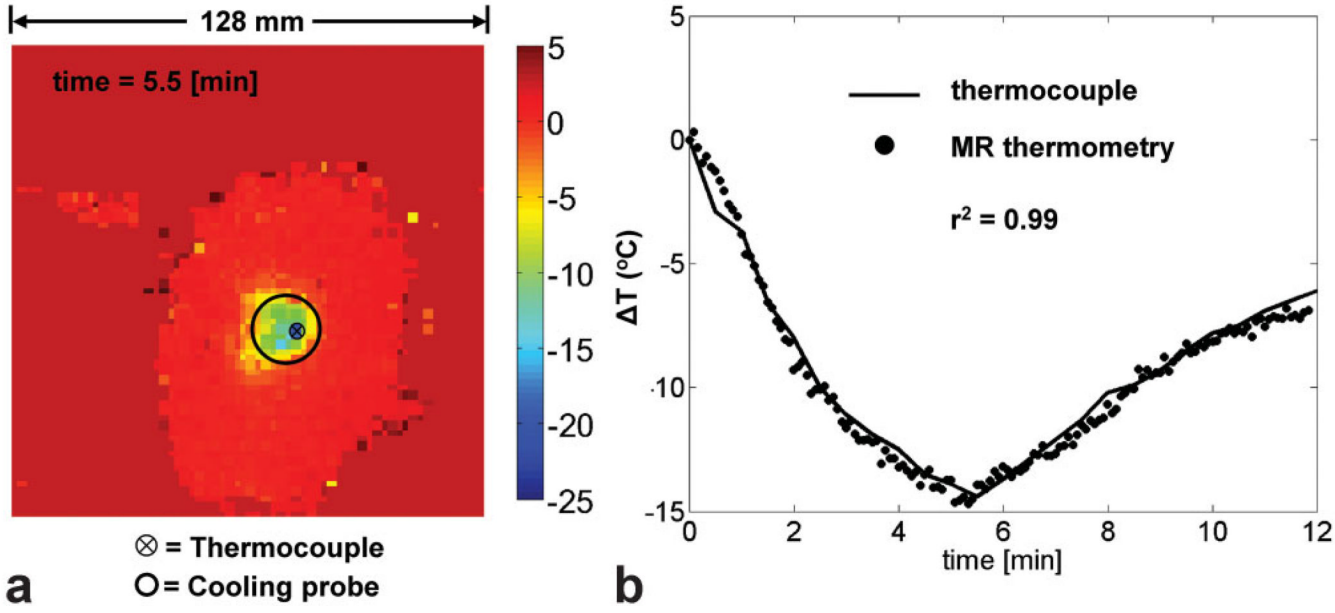

FIG. 2.

a: MR-defined temperature map during cooling of ex vivo bovine muscle (5.5 min after start of cooling). The location of the probe is indicated by the black circle and the location of the thermocouple under the probe by the circle with an "x" inside. **b:** Plot of MR thermometry measurements (average of four voxels) versus thermocouple readings during the cooling and recovery stages of the experiment. Both images show the change in temperature from room temperature (22°C).

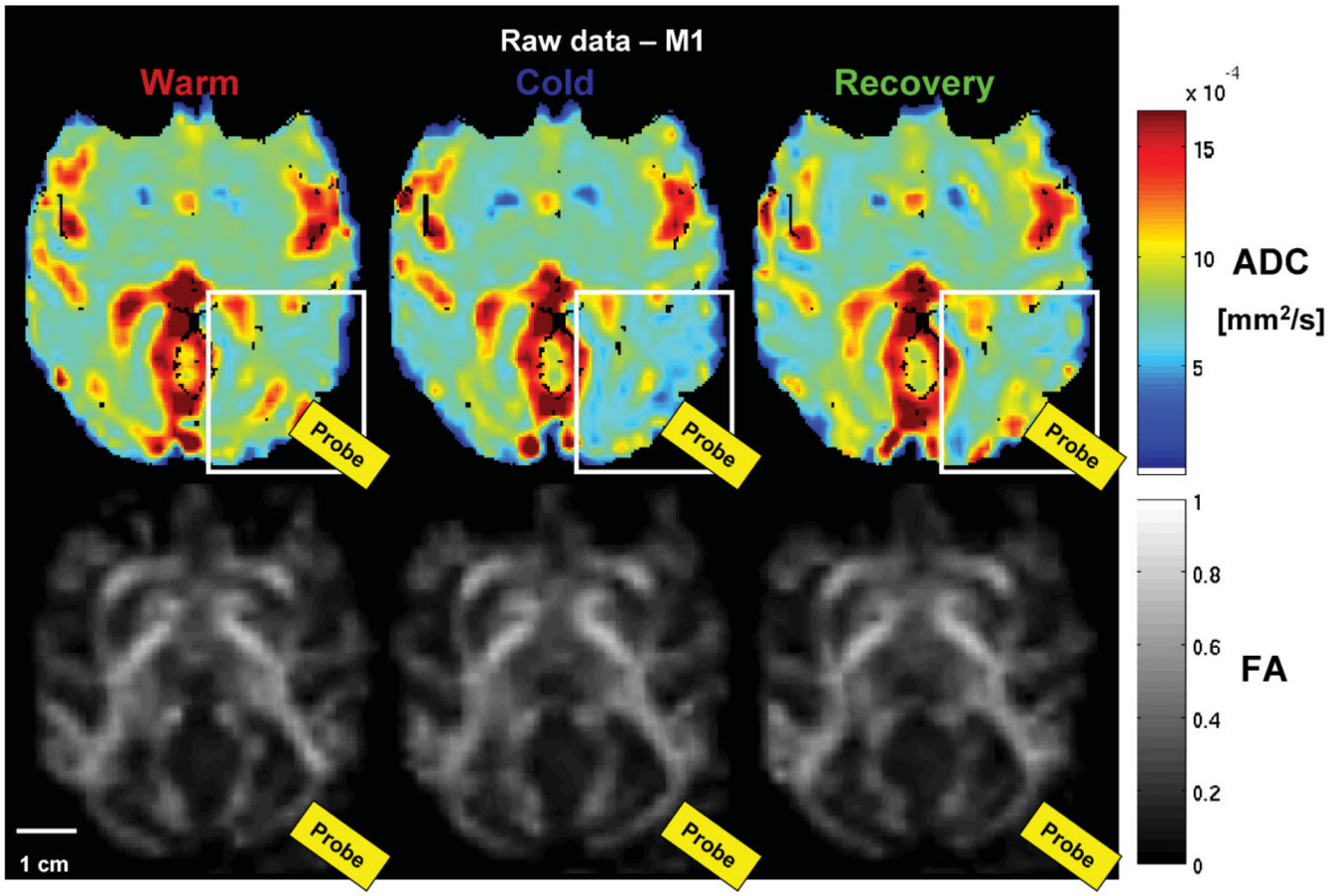

FIG. 3.

Epoch-averaged ADC (top row) and FA maps (bottom row) for the warm, cold, and recovery conditions for an experiment where the temperature under the probe = 8°C (cortical deactivation #1, M1). The change in ADC is apparent under the probe (white rectangle) during the cold condition, however, no change in the FA is visible.

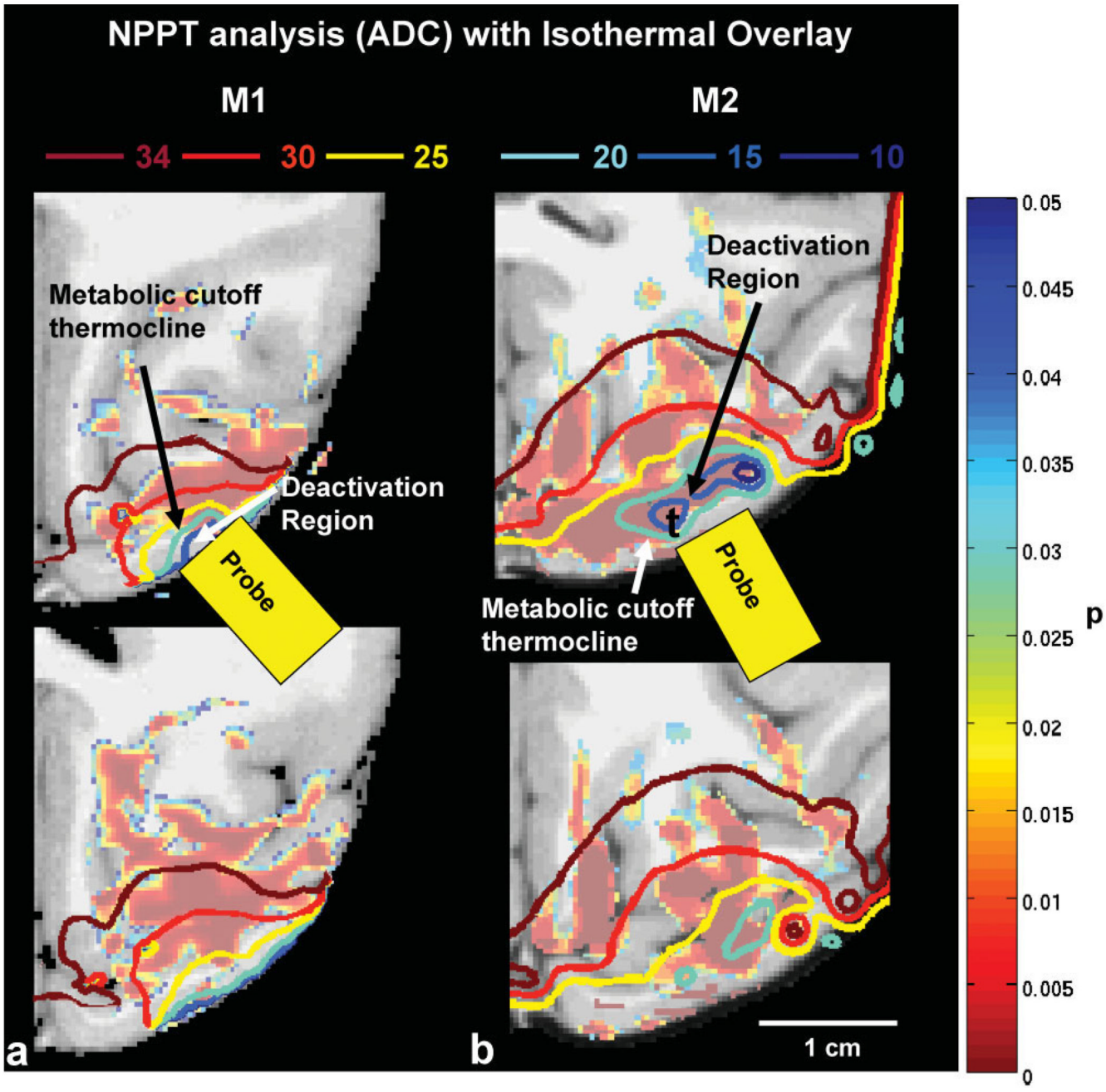

FIG. 4.

a,b: Region where ADC changed significantly ($P < 0.05$) between the warm and recovery conditions versus the cold condition as calculated by NPPT for (A) M1 and (B) M2. Isothermals at 34, 30, 20, 15, 10°C were overlaid on the images. Note that the statistically significant region extends beyond the cooled region and is present where the temperature has not changed significantly from the body temperature (T > 34°C isothermal).

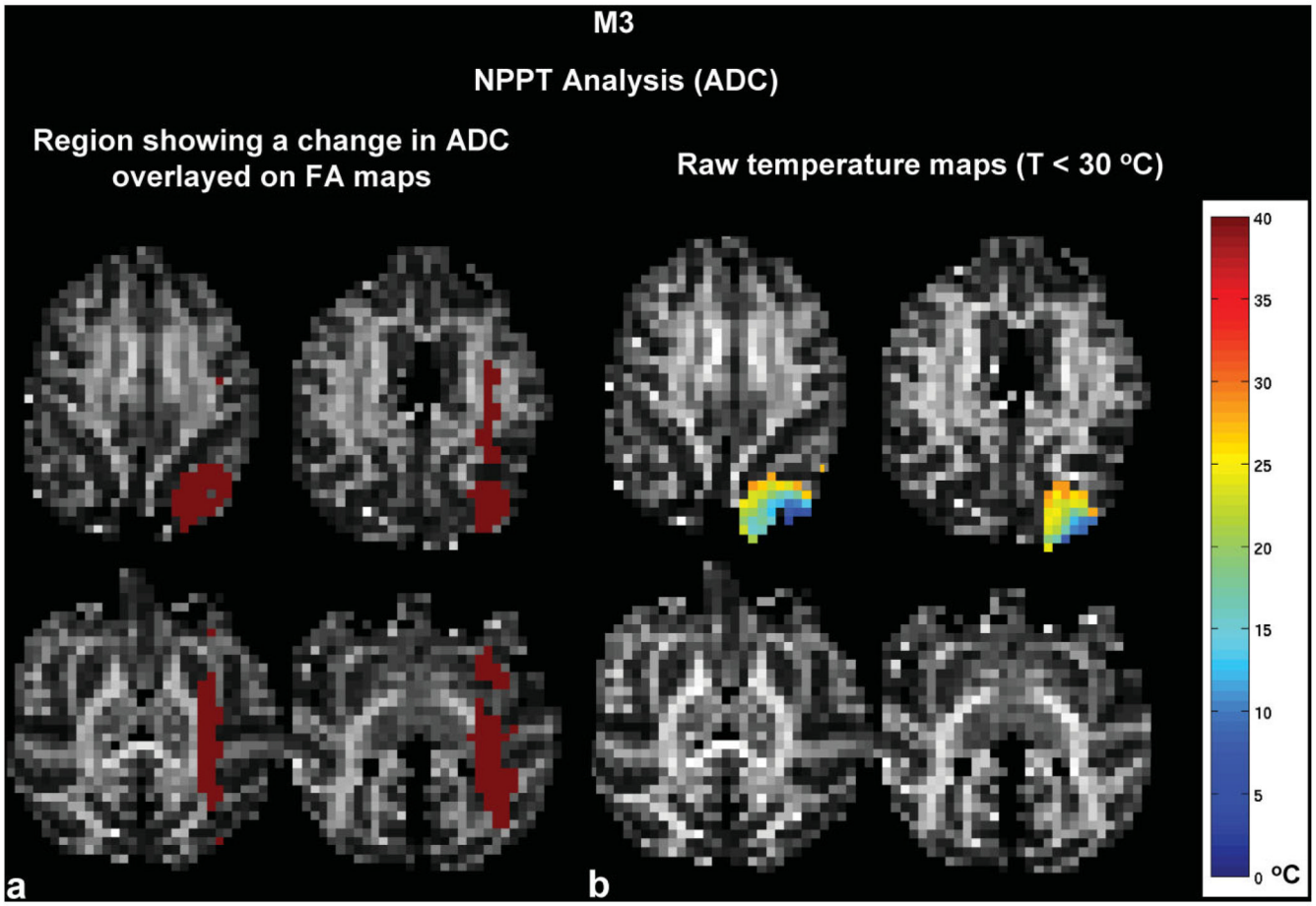

FIG. 5.

a,b: Raw data from M3 showing the (A) region where the ADC changed (in red) as calculated from the NPPT analysis and (B) raw temperature maps (T < 30°C). The region where the ADC decreased extended far beyond the cooling region.

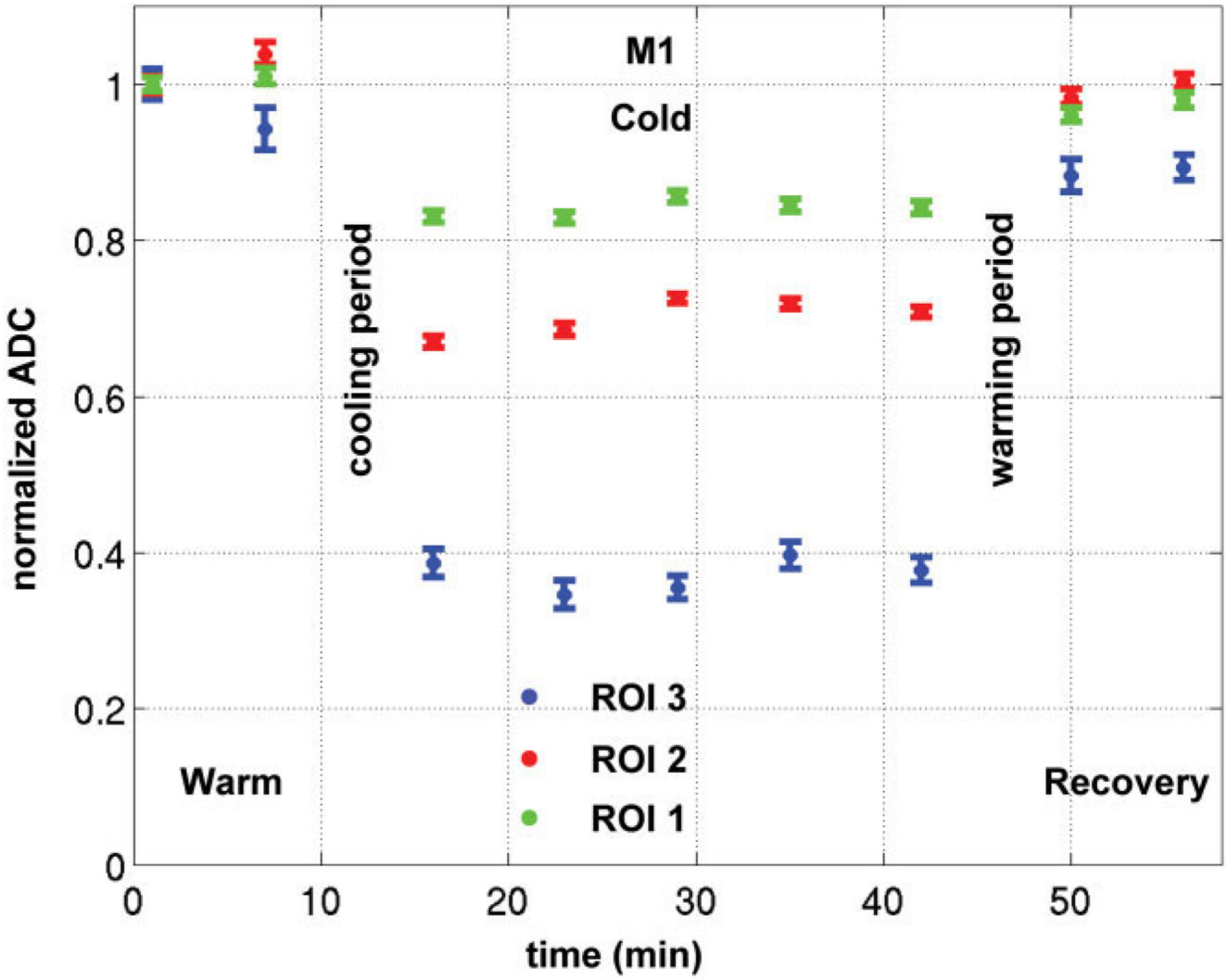

FIG. 6.

Plot of the mean normalized ADC (± SEM) in M1 versus time in three temperature ranges: 8–20°C (ROI 3), 20–34°C (ROI 2), 34–40°C (ROI 1). The ADC was normalized relative to the first warm image for each ROI. The consistent ADC decrease in function of time during the cold condition indicates the brain was already deactivated at the beginning of the cold DTI scans and that the temperature remained constant in each region.

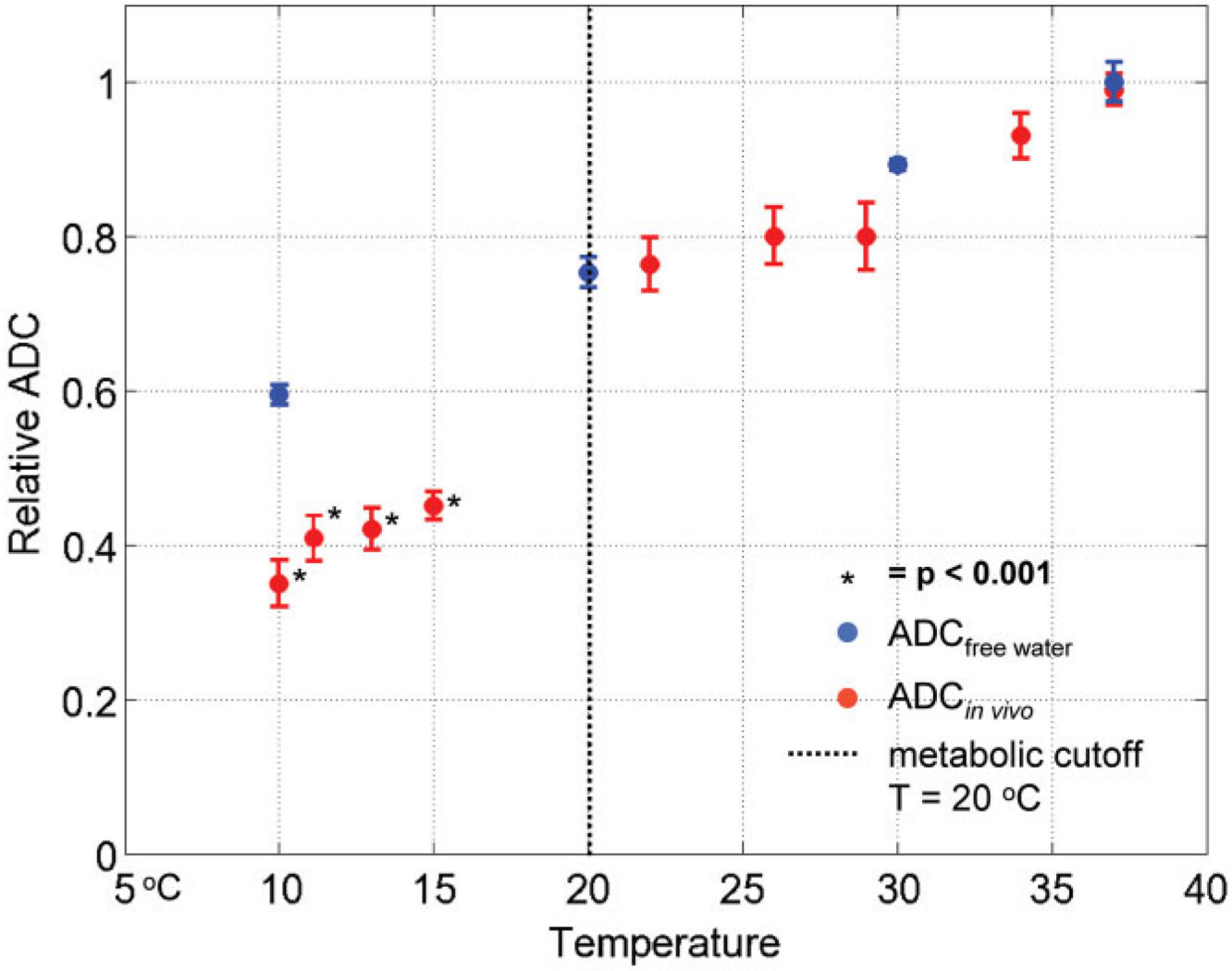

FIG. 7.

The normalized in vivo ADC ($ADC_{in\ vivo}$, red) and the normalized ADC of free water ($ADC_{free\ water}$, blue) (32,33) plotted as a function of temperature for the nine reversible deactivation experiments. The deactivated region, T < 20°C (ROI 1), from M1, M2 and M3 was used to compare the ADC between the nine reversible deactivation experiments. Note the $ADC_{in\ vivo}$ follows the diffusion of free water for T > 20°C, but not below the metabolic cutoff. $ADC_{in\ vivo}$ values with an asterisk are statistically significant *P*-values (alpha level = 0.001) from a one sample t-test comparing the difference between the normalized $ADC_{in\ vivo} - ADC_{free\ water}$ (see Table 2).

Table 1

Percent Change in ADC (± SEM) Relative to the First Warm ADC Value for Three Temperature Ranges (34–40°C, 20–34°C, 8–20°C) During the Warm, Cold, and Recovery Conditions*

Region	M1						M2					
	Gray			White			Gray			White		
	34–40 °C						34–40 °C					
	W	**C**	**R**	**W**	**C**	**R**	**W**	**C**	**R**	**W**	**C**	**R**
ROI 1	−0.12 ± 0.95	**−18.69 ± 0.59 (6e-6)**	−4.85 ± 0.68	1.05 ± 2.12	**−11.95 ± 0.31 (2e-6)**	2.25 ± 1.73	−0.45 ± 0.75	**−21.18 ± 3.06 (9e-4)**	3.05 ± 3.66	0.49 ± 0.82	**−19.33 ± 2.51 (6e-5)**	6.57 ± 2.41
	20–34 °C						20–34 °C					
Region	W	C	R	W	C	R	W	C	R	W	C	R
ROI 2	0.45 ± 0.46	**−40.90 ± 0.78 (3e-8)**	0.55 ± 2.4	−0.85 ± 2.01	**37.00 ± 1.07 (4e-7)**	3.81 ± 3.63	−0.9 ± 2.4	**−42.02 ± 1.67 (3e-8)**	−3.23 ± 2.68	−0.65 ± 1.75	**−41.76 ± 1.07 (7e-8)**	−0.19 ± 3.91
	8–20 °C						8–20 °C					
Region	W	C	R	W	C	R	W	C	R	W	C	R
ROI 3	0.54 ± 1.45	**−54.3 ± 1.77 (8e-5)**	−7.14 ± 2.9	1.01 ± 2.75	**−54.58 ± 2.82 (1e-5)**	−14.67 ± 3.03	1.4 ± 3.2	**−67.5 ± 3.01 (1e-8)**	−5.99 ± 2.94	1.34 ± 2.45	**−62.58 ± 2.82 (2e-9)**	−20.67 ± 3.68

M3					
Gray			White		
34–40 °C					
W	C	R	W	C	R
0.53 ± 0.32	**−21.98 ± 0.83 (5e-6)**	5.45 ± 1.82	0.84 ± 0.48	**−19.84 ± 0.72 (8e-7)**	3.76 ± 1.95
20–34 °C					
W	C	R	W	C	R
0.67 ± 0.45	**−36.17 ± 2.15 (4e-6)**	−1.75 ± 2.34	0.23 ± 0.52	**−38.45 ± 2.01 (7e-6)**	1.20 ± 2.92
8–20 °C					
W	C	R	W	C	R
0.71 ± 0.82	**−58.65 ± 2.75 (1e-6)**	−7.45 ± 2.87	−0.23 ± 0.65	**−57.43 ± 2.91 (3e-5)**	−8.65 ± 3.31

*The values in parenthesis are statistically significant *P* values ($P < 0.001$) from a one sample t-test.

Table 2

Normalized $ADC_{\text{in vivo}}$ − *normalized* $ADC_{free\ water}$ *(± SEM) as a function of temperature**

Average temperature ROI 1 (° C)	**10**	**10.5**	**13**	**15**	**22**	**26**	**29**	**34**	**37**
$ADC_{in\ vivo} - ADC_{free\ water}$	**−24.50 ± 2.00 (2e-6)**	**−20.45 ± 2.82 (3e-4)**	**−22.24 ± 4.00 (8e-5)**	**−22.41 ± 3.60 (6e-5)**	−1.70 ± 4.30	−3.67 ± 3.70	−7.85 ± 4.32	−2.39 ± 2.90	1.00 ± 2.13

The values in parenthesis are statistically significant *P* values (alpha level = 0.001) from a one sample t-test.